Materials Science & Engineering A 644 (2015) 90–95

Contents lists available at ScienceDirect

Materials Science & Engineering A

journal homepage: www.elsevier.com/locate/msea

Fabrication and properties of graphene reinforced silicon nitride composite materials

Yaping Yang, Bin Li*, Changrui Zhang, Siqing Wang, Kun Liu, Bei Yang

Science and Technology on Advanced Ceramic Fibers and Composites Laboratory, College of Aerospace Science and Engineering, National University of Defense Technology, Changsha 410073, PR China

ARTICLE INFO

Article history:
Received 27 May 2015
Received in revised form
6 July 2015
Accepted 21 July 2015
Available online 21 July 2015

Keywords:
Graphene
Silicon nitride ceramics
Hot pressing
Pressureless sintering
Mechanical properties

ABSTRACT

Silicon nitride (Si_3N_4) ceramic composites reinforced with graphene platelets (GPLs) were prepared by hot pressed sintering and pressureless sintering respectively. Adequate intermixing of the GPLs and the ceramic powders was achieved in nmethyl-pyrrolidone (NMP) under ultrasonic vibration followed by ball-milling. The microstructure and phases of the Si_3N_4 ceramic composites were investigated by Field Emission Scanning Electron Microscopy (SEM) and X-ray diffraction (XRD). The effects of GPLs on the composites' mechanical properties were analyzed. The results showed that GPLs were well dispersed in the Si_3N_4 ceramic matrix. β-Si_3N_4, O′-sialon and GPLs were present in the hot-pressed composites while pressureless sintered composites contain β-Si_3N_4, Si, SiC and GPLs. Graphene has the potential to improve the mechanical properties of both the hot pressed and pressureless sintered composites. Toughening effect of GPLs on the pressureless sintered composites appeared more effective than that on the hot pressed composites. Toughening mechanisms, such as pull-out, crack bridging and crack deflection induced by GPLs were observed in the composites prepared by the two methods.

© 2015 Elsevier B.V. All rights reserved.

1. Introduction

Silicon nitride, an advanced ceramic material, is considered suitable for structural applications including high speed cutting tools, chemical and electrical insulators and various coatings due to its excellent mechanical properties at both room and elevated temperatures, good thermal shock resistance and excellent ablation resistance. However, because of the intrinsic brittleness of ceramic materials, it is crucial to improve the strength and toughness of silicon nitride ceramics to make them more reliable for engineering applications [1–6]. Reinforcing ceramic materials with appropriate nanofillers will significantly improve their strength and toughness, as well as electrical and thermal properties. These nanofillers can provide a variety of extrinsic toughening mechanisms [7–14].

For instance, carbon nanotubes (CNTs) with high tensile strength, good flexibility, and low density have been widely investigated as nanofillers to improve the electrical and thermal conductivity of the host materials with low filler contents. The enhancement of properties such as electrical conductivity and elastic modulus has been observed in polymer composites containing CNTs [11]. Balázsi et al. [12] fabricated the CNT–Si_3N_4 composites by spark plasma sintering (SPS) and a 25% increase in fracture toughness was achieved, compared to monolithic Si_3N_4. Bocanegra Bernal et al. [13] studied the effects of carbon nanotubes on the properties of ZrO_2 toughened Al_2O_3 (ZTA) composites and reported a 44% increase in fracture toughness over the pure ZTA.

Recently discovered graphene is a one atom thick 2-D layer of sp [2] carbon arranged in a honeycomb lattice [15,16], which has imposed itself with many unique outstanding properties. These properties make graphene a promising candidate of nanofiller material in various applications. The intrinsic mechanical properties of graphene reported so far, such as Young's modulus of 1 TPa and ultimate strength of 130 GPa, make it one of the strongest materials available [17–19,35]. Moreover, graphene is considered to have unusual electrical properties [20–22,35] and high thermal properties [23,24,35]. It has been shown that a single graphene layer is a zero-gap semiconductor with a linear Dirac-like spectrum around the Fermi energy, which manifests graphene in unusual phenomena such as an anomalous quantum Hall effect. Graphene has very high thermal conductivity *K*. The first experimental determination of the thermal conductivity of suspended monolayer graphene pegged the value at 5300 $W\,m^{-1}\,K^{-1}$ and a phonon mean free path of 775 nm near room temperature. Due to its remarkable properties, graphene has been selected as the nanofiller in a multitude of studies. It has been demonstrated in some studies that a relatively low addition of graphene to various

* Corresponding author. Fax: +86 731 84576578.
E-mail address: libin@nudt.edu.cn (B. Li).

http://dx.doi.org/10.1016/j.msea.2015.07.062
0921-5093/© 2015 Elsevier B.V. All rights reserved.

ceramic based composites could result in a substantial improvement of electric, thermal and mechanical properties [25–34]. Liu et al. [31] used spark plasma sintering (SPS) to prepare Al_2O_3–graphene composite. A 27.20% increase in fracture toughness and a 30.75% increase in flexural strength were obtained with 0.78 vol% GPLs. Walker et al. [30] employed aqueous colloidal processing to obtain uniform and homogeneous dispersions of GPLs and Si_3N_4 ceramic particles which were then densified by SPS. The measured fracture toughness of monolithic Si_3N_4 (2.8 MPa $m^{1/2}$) increased to 6.6 MPa $m^{1/2}$ by 235% with 1.5 vol% GPLs.

In this study, we focus on the preparation of silicon nitride composites reinforced with GPLs by two different methods, hot pressed sintering and pressless sintering. Microstructures of the GPLs reinforced Si_3N_4 composites fabricated by the two methods were investigated and analyzed using Field Emission Scanning Electron Microscopy (SEM). Components of the composites were characterized using X-ray diffraction (XRD). Density and mechanical properties, including flexural strength and fracture toughness of the ceramic composites, were measured. The effect of GPLs contents on the mechanical properties of the ceramic composites prepared by the two methods was compared and discussed.

2. Experimental procedure

2.1. Preparation process

The starting powder mixture used for the fabrication of composite materials consists of α-Si_3N_4 powder (supplied by Xingrongyuan Technology Co. Ltd., Beijing, China) with a purity of 99.9% and an average particle size of 2 mm, sintering additives (5 wt% Y_2O_3, 2 wt% Al_2O_3 and 1 wt% MgO) and filler material graphene (G-100, purchased from Shanghai Simbatt Energy Technology Co. Ltd.). N-methyl pyrrolidone (NMP) solvent from Aladdin Industrial Corporation was also purchased. The powders were blended to obtain mixtures containing 0, 0.2, 0.5, 1, 2, 5 and 10 wt% of GPLs. The GPLs and α-Si_3N_4 particles were dispersed in NMP solvent by bath sonication for half an hour, followed by a ball milling procedure at 400 rpm in a planetary ball mill for 12 h. Such a high filling of the milling chamber aimed at well dispersing and destroying graphene agglomerates. The milled slurry mixture was extracted through the sintered-glass filter funnel to pump out the solvent and then the as-received mixture was dried under 120 °C in an oven for 24 h. Finally the dried powder mixture was ground and sieved using a 120 mesh sieve.

Bulk composite samples were sintered through hot pressed sintering process and pressureless sintering process respectively. In the process of hot pressing, the powder mixtures were poured into a graphite mold of 70 mm in diameter. Graphitic papers with 1 mm thick were placed between the powder and the mold or punch and the powder for easy removal of the sintered samples. The preforms in the graphite mold were heated to 1200 °C for 1 h and then elevated to the maximum temperature of 1750 °C in 1 h. Next the composites were heat treated at 1750 °C for 1 h and then cooled down to the room temperature with the furnace. The whole process was carried out in a nitrogen flow under a uniaxial pressure of 20 MPa. Sintered composites with a dimension of 30 mm × 40 mm × 5 mm were obtained. The temperature was measured and controlled using an optical pyrometer. Shrinkage, displacement, heating current, and voltage were also recorded during the sintering processes.

In the process of pressureless sintering, the powder mixture were cold-pressed into the preforms with a dimension of 40 mm × 40 mm × 5 mm which were then packaged, vacuumized and cold isostatically pressed at 150 MPa in the cold isostatic press (KJYS-200). After that, the preforms were sintered in a nitrogen flow at atmospheric pressure. The temperature program of the pressless sintering was the same as hot pressing process. Sintered specimens with a dimension of 40 mm × 40 mm × 5 mm were obtained.

2.2. Characterization and tests

Density of the ceramic composites was measured by Archimedes' method and relative density was calculated by dividing bulk density with the theoretical density of the powder mixture. Microstructure and morphology of the surfaces and fractures of Si_3N_4–graphene composites were observed by scanning electron microscopy (SEM, Sirion200). X-ray diffraction (XRD, ADVANCED D8) were carried out in order to obtain the components of the obtained ceramic composites.

Flexural strength of the composites was measured via three-point bending test (WDW-100) with a span length of 30 mm and a loading speed of 0.5 mm/min and, five rectangular specimens with a dimension of 35 mm × 4 mm × 3 mm were tested to obtain an average strength. Fracture toughness (K_{IC}) of the composites was measured by single edge notched beam method. Five specimens with a dimension of 30 mm × 2.5 mm × 5 mm were tested to obtain the average toughness.

3. Results and discussion

3.1. Microstructure characterization

The high stability exhibited by GPLs/NMP dispersions allows the homogeneous mixing of GPLs (< 5 nm in thickness) with Si_3N_4 powders via sonication and ball milling. Following the solvent extraction through sintered-glass filter funnel, the Si_3N_4–graphene intermixing was preserved, as illustrated in Fig. 1a, which shows that the graphene flakes were well dispersed in the matrix powders.

The sintered ceramic composites were fractured and their micro-structures were examined. Fig. 1b–d show the SEM images of fracture surfaces of the composites with GPLs. Upon hot pressing, the graphene sheets remain relatively flat (see inset in Fig. 1b). Meanwhile, there were often two or more GPLs stuck closely together. These multi-platelets tended to be distributed intergranularly in the matrix grain boundaries and were often connected with some porosity, which can prevent the migration of the grain boundaries. While in the process of pressureless sintering, single graphene sheets were tucked and wrapped around the matrix grains, as is shown by the arrows in Fig. 1d. Besides, pores were frequently observed and the edges of the graphene platelets tend to scroll, even formed tubular structures (see inset in Fig. 1c and d). The two-dimensional structures of graphene have been postulated to be intrinsically unstable because long-wavelength fluctuations destroy the long-range order of 2-D crystals according to the Mermin–Wagner theorem [35]. It is the intrinsic microscopic undulations that have contributed to the stability of the suspended 2-D graphene sheets. Therefore, this kind of 2-D crystal embedded in 3-D space has a tendency to crumple [35]. Thus, in the process of pressureless sintering, ubiquitous tubular structures within the residual pores as well as the undulations imposed by the Si_3N_4 substrate surface morphology can be observed. Compared to the pressureless sintering process, the load applied to the die containing the Si_3N_4–graphene mixtures during hot pressing enabled the stability of the flat morphologies, thus leading to less porosity and avoiding the scrolling of the graphene sheets edges. In addition, the homogeneous distribution of the GPLs was well preserved by the constant load throughout densification.

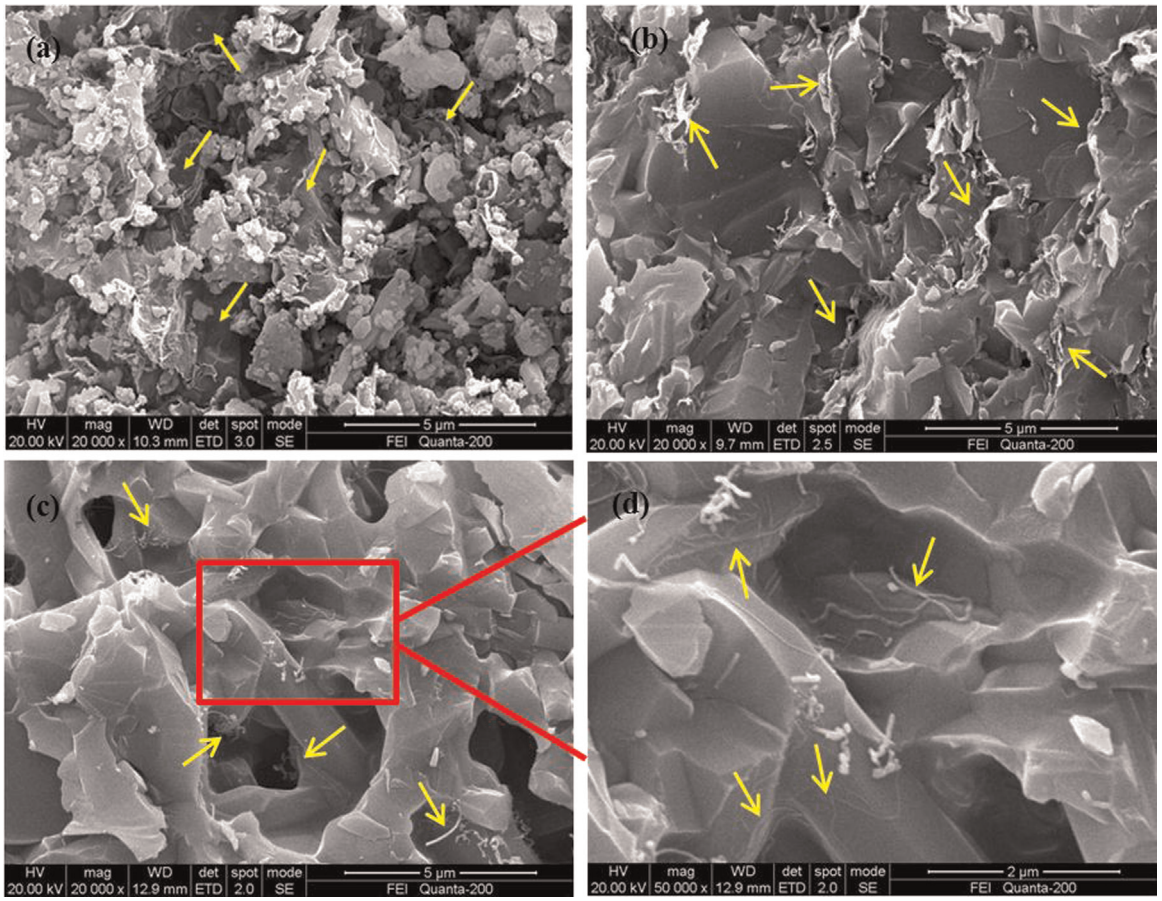

Fig. 1. Fracture surfaces of the sintered composites. (a) The Si_3N_4–graphene mixture powders. (b) The composites fabricated by hot pressing. (c, d) The composites fabricated by pressureless sintering. The arrows indicate GPLs embedded in the matrix.

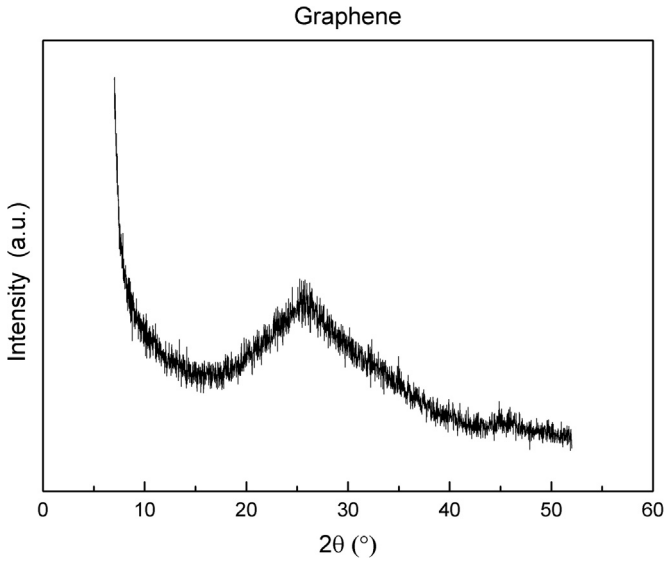

Fig. 2. XRD pattern of pure graphene platelets.

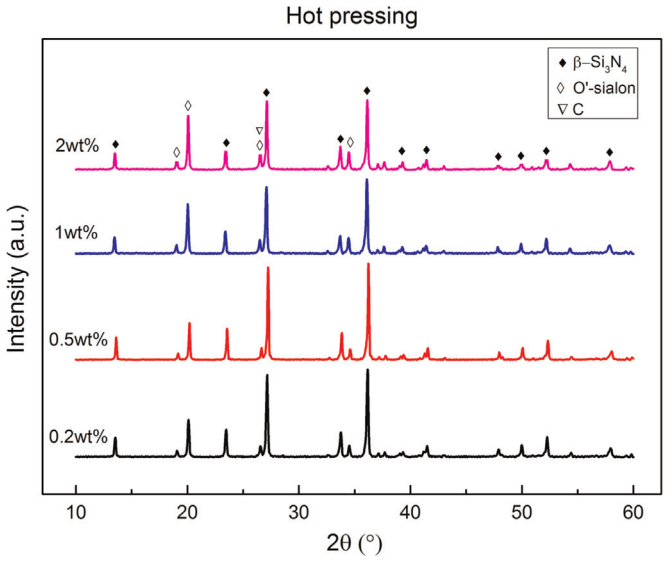

Fig. 3. XRD patterns of the composites fabricated by hot pressing with different weight percentage of GPLs.

The XRD pattern of pure graphene platelets (Fig. 2) shows that the characteristic peak of graphene is at 26.6°. The difficulty of preparing smooth samples of GPLs for XRD characterization has attributed to the gentle and rough characteristic peak. In all the hot pressed composites, the characteristic peak of graphene at 26.6° can be identified distinctly, which also indicates that the graphene flakes can exist stably in the Si_3N_4 substrate. Figs. 3 and 4 show the XRD patterns of the hot pressed and pressureless sintered Si_3N_4–graphene composites fabricated with 0.2–10 wt% graphene. The process of sintering at 1750 °C resulted in the crystallization of amorphous powder during sintering. Diffraction peaks at 2θ value of 13.4°, 23.4°, 27.1°, 33.7°, 36.1°, 41.4°, 52.2° correspond to the dominant phase, β-crystalline Si_3N_4, and no residual α-Si_3N_4 could be detected from the XRD data, suggesting the full transformation from α-Si_3N_4 to β-Si_3N_4. Peaks of O′-sialon

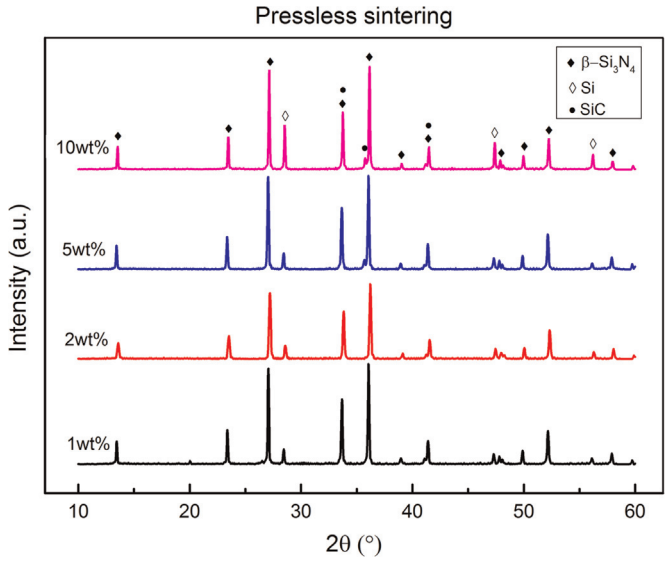

Fig. 4. XRD patterns of the composites fabricated by pressureless sintering with different weight percentage.

were observed in hot pressed composites (Fig. 3), while in pressureless sintered composites, there existed Si and SiC and no prominent peaks of O′-sialon and graphene were found (Fig. 4). It is known that the sintering additives react with the SiO_2 that is present at the surface of the Si_3N_4 starting powder to form a liquid phase during sintering. Subsequently, the α-Si_3N_4 particles dissolve in this liquid phase, causing a local supersaturation and re-precipitation of β-Si_3N_4. In the process of transformation of Si_3N_4 from α- to β-structure, Al^{3+} and O^{2-} ions could enter the β-Si_3N_4 structure to replace some Si^{4+} and N^{3-} ions respectively, and formed the O′-sialon solid solution [36]. Upon cooling, the liquid phases formed during sintering devitrify partially or totally. The remainder solidifies as an intergranular glass phase which cannot be identified through XRD patterns. During pressureless sintering, without the uniaxial pressure, the fluidity of the liquid phase was higher and graphene sheets were more flexible. The graphene sheets wrapped the Si_3N_4 grains and the Si^{4+} ions have partially reacted with graphene to form SiC. The dissociated Si left unreacted explained the existence of residual Si. With the absence of uniaxial pressure, the liquid phase probably has not devitrified totally during the pressureless sintering, therefore no prominent peaks of O′-sialon and graphene were found.

3.2. Density

Generally, the density of a bulk sample indicates how effectively the sample has been processed. Bulk mechanical properties are usually affected by sample density. Denser composites are therefore desired for ceramic materials as pores within them would act as defects and lower strength. The bulk densities and relative densities of the hot pressed and pressureless sintered composites with and without GPLs are plotted in Fig. 5a and b. Relative densities of the Si_3N_4–graphene composites were calculated using the rule of mixture equation, assuming that the absolute density of β-Si_3N_4 is 3.2 g/cm [3].

Fig. 5a and b show that the material density and relative density of the composites fabricated by hot pressing and pressureless sintering increased with graphene fraction at the beginning and then showed a decreasing trend. For hot pressed composites, both the density and relative density of the composites prepared with 0.2 wt% graphene reached a maximum and, there was a 1.4% increase in density compared to monolithic Si_3N_4. While for pressureless sintered composites, the maximum bulk density and relative density were at the content of 2 wt% graphene and, the density has increased by 5%.

In both of the two sintering processes, with the sintering temperature up to 1750 °C, volume diffusion enhanced, resulting in full densification. A fraction of fillers also facilitated the densifying process. However, the presence of excessive graphene could lower the effective material density. On one hand, graphene is significantly less dense than Si_3N_4 and the density of graphene is lower compared to crystalline Si_3N_4. Thus, the overall bulk density of the composites should be lower. On the other hand, the bulk density was also affected by the porosity in the composites. With the increasing of graphene fraction, graphene platelets tended to aggregate, inducing more pores forming in the interface between GPLs and ceramic matrix due to the degraded flexibility of the aggregated GPLs. Compared to the hot pressed composites, the pressureless sintered composites were less dense. This is because without the uniaxial pressure, more pores would form between the matrix grains. Graphene's enhancement effects on the density of the pressureless sintered composites were more remarkable than that of the hot pressed composites.

3.3. Mechanical properties

Flexural strength and fracture toughness of the Si_3N_4–graphene composites fabricated by the two methods are shown in Fig. 5c–f. Both the values of flexural strength and fracture toughness of the composites rose and then decreased with the increasing of the graphene fraction, which was in accordance with the trend of the composite density. For hot pressed composites, the flexural strength increased slightly by 3.1% and the fracture toughness increased by 10.2%, while for pressureless sintered composites, there was a 147% increase in flexural strength and a 30.3% increase in fracture toughness. Both of the maximum values of the flexural strength and fracture toughness of the hot pressed composites were achieved with 0.2 wt% graphene and, the pressureless sintered ones were with 2 wt% graphene, the same amount as that of the maximum values of density. It is normal that the bulk strength and toughness of hot pressed composites were higher than that of the pressureless sintered composites since the former composites were denser than the latter ones. The toughness and strength increases in hot pressed composites seemed to be within the error of the measurement. However, these increases were more significant in pressureless sintered composites.

Toughening mechanisms including pull-out, crack bridging and crack deflection, were observed in both the hot pressed and pressureless sintered composites. When consolidation proceeded during the sintering process, graphene sheets were embedded within the grain boundaries of the matrix in hot pressed composites (Fig. 1b) and wrapped the matrix grains in pressureless sintered composites, resulting in the increased interface strength between GPLs and Si_3N_4 matrix. On one hand, flexural strength and fracture toughness of the ceramics were therefore improved due to the increased energy of pulling out the graphene sheets from the grain boundaries. In addition, GPLs can hinder crack propagation and deflect cracks, creating other tortuous paths to release stress, which helps increase the strength of the composites. However, on the other hand, in the process of hot pressing, with the uniaxial pressure, the existence of graphene in the matrix can be a hindrance to the diffusion and mass transport of material across the grain boundaries during long periods of time at elevated temperatures, resulting in less efficient strengthen effects of graphene. This did not happen in the process of pressureless sintering since the growth of the matrix grains were not constrained without the load applied to the Si_3N_4–graphene mixtures. Moreover, the presence of Intergranular phase O′-sialon solid solution

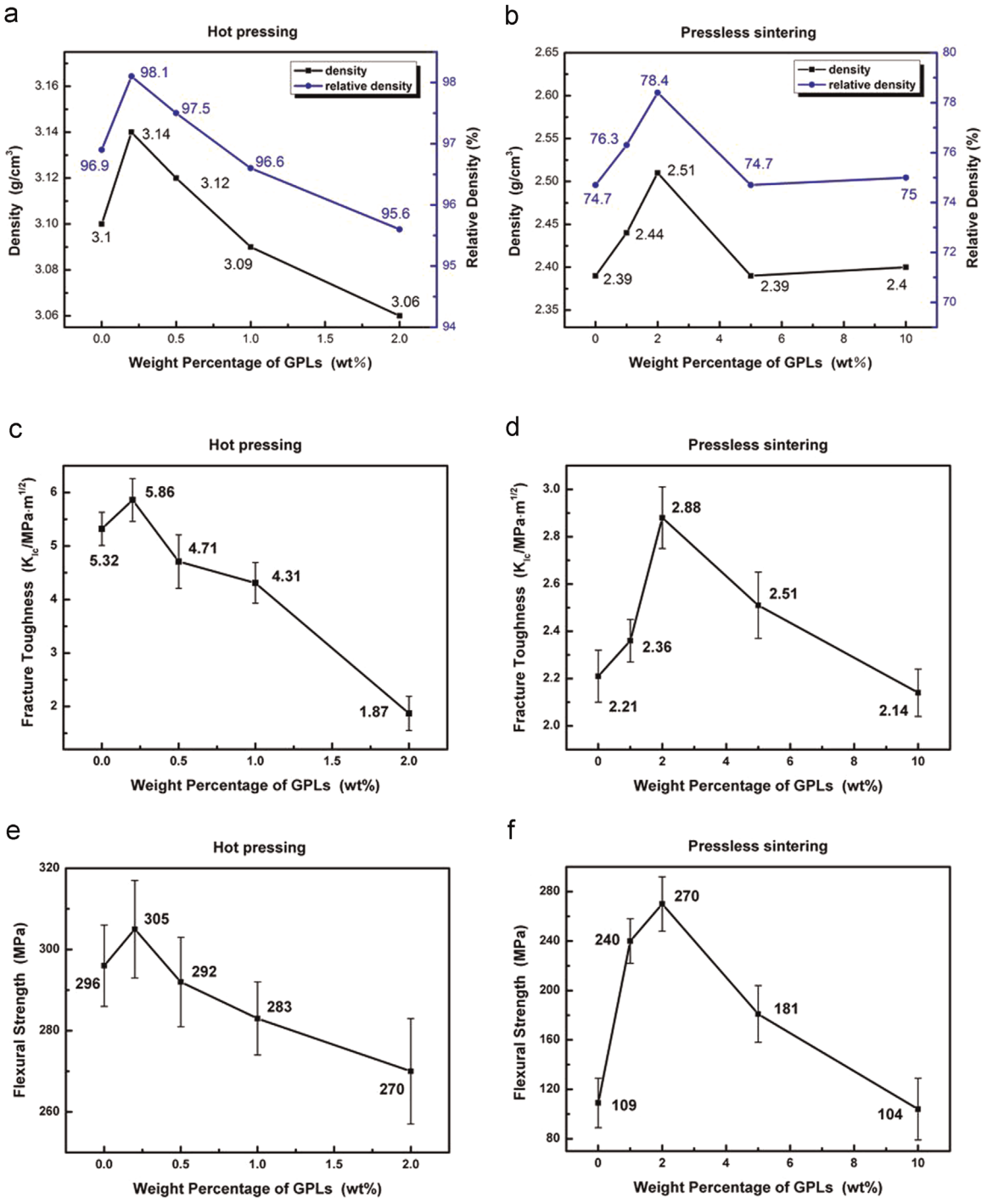

Fig. 5. (a, b) Density and relative density of the hot pressed and pressureless sintered Si_3N_4–graphene composites with different weight percentage of GPLs. (c, d) Fracture toughness of the hot pressed and pressureless sintered Si_3N_4–graphene composites with different weight percentage of GPLs. (e, f) Flexural strength of the hot pressed and pressureless sintered Si_3N_4–graphene composites with different weight percentage of GPLs.

(Fig. 3) in hot pressed composites was another factor that may explain why there was just a slight increase in the bulk toughness and strength. Intergranular phases generally have thermal expansion coefficients different to that of Si_3N_4 grains so that the grain boundary phase is under tensile stress at room temperature after sintering.

The obtained results showed that the addition of more than 2 wt% and 0.2 wt% of graphene in pressureless sintered and hot pressed composites respectively, caused a noticeable decrease in the bulk mechanical properties. For pressureless sintered composites, the higher the concentration of graphene was, the larger the chances of the reaction between graphene and the dissociated monatomic Si (as shown in Fig. 4) were, which caused the weak boundaries between the silicon nitride matrix and graphene. Besides, dispersion level of the nanostructures in matrix is also one of the key factors in defining the mechanical properties of the composites since graphene has a strong tendency towards agglomeration especially when its content increases. The presence of aggregation leads to more residual pores in the interface between GPLs and the ceramic matrix, causing the mechanisms of pull-out, crack bridging and crack deflection to function in a less efficient way, which explains the fact that an excessive addition of GPLs led

to less strong composites for both the hot pressed and pressureless sintered composites. To further increase the density, improvement in the exfoliation level of the starting material and the exfoliation efficiency during the milling process would be needed. In a whole, an optimum percentage of GPLs in the composites can result in the maximum flexural strength and fracture toughness.

4. Conclusions

Si_3N_4 ceramic composites containing well distributed graphene platelets were successfully prepared by hot pressed sintering and pressureless sintering. NMP dispersion and ball milling produced a high exfoliation and uniform distribution of graphene platelets within the starting powder mixture. SEM patterns showed that GPLs were well dispersed in the Si_3N_4 ceramic matrix. The uniaxial pressure during hot pressing avoided the scrolling of the graphene sheets edges, whereas in pressless sintering, graphene sheets have formed tubular structures. XRD analyses indicated the presence of O′-sialon in hot pressed composites except for the dominant phase β-Si_3N_4, yet in pressureless sintered composites, graphene has partially reacted with the Si_3N_4 matrix. In hot pressing, well densified composites were obtained while pressureless sintered composites were less dense. There was an increase by 3.1% in flexural strength (304.91 MPa) and an increase by 10.2% in fracture toughness (5.86 MPa $m^{1/2}$) respectively with 0.2 wt% GPLs for hot pressed composites. Nevertheless, for pressureless sintered composites the strengthen effect appeared more significant. With 2 wt% GPLs, the flexural strength (270 MPa) increased by 147% and fracture toughness (2.88 MPa $m^{1/2}$) increased by 30.3% respectively. Toughening mechanisms of pull-out, crack bridging and crack deflection were observed in both the composites fabricated by the two methods. These findings indicated that graphene had the potential to improve the strength of the composites, and a more appropriate way to prepare light and strong ceramic composites to suit engineering applications.

Acknowledgment

The financial supports by Aid Program for Science and Technology Innovation Research Team in Higher Educational Institution of Hunan Province, Aid Program for Innovative Group of National University of Defense Technology are gratefully acknowledged.

References

[1] Y.F. Xia, Y.P. Zeng, D.L. Jiang, Microstructure and mechanical properties of porous Si_3N_4 ceramics prepared by freeze-casting, Mater. Des. 33 (2012) 98–103.
[2] C.R. Zou, C.R. Zhang, B. Li, Microstructure and properties of porous silicon nitride ceramics prepared by gel-casting and gas pressure sintering, Mater. Des. 44 (2013) 114–118.
[3] Y. Inagaki, N. Kondob, T. Ohji, High performance porous silicon nitrides, J. Eur. Ceram. Soc. 22 (2002) 2489–2494.
[4] Y.F. Xia, Y.P. Zeng, D.L. Jiang, Dielectric and mechanical properties of porous Si_3N_4 ceramics prepared via low temperature sintering, Ceram. Int. 35 (2009) 1699–1703.
[5] J.F. Yang, Z.Y. Deng, T. Ohji, Fabrication and characterisation of porous silicon nitride ceramics using Yb_2O_3 as sintering additive, J. Eur. Ceram. Soc. 23 (2003) 371–378.
[6] Y.H. Koh, H.W. Kim, H.E. Kim, J.W. Halloran, Thermal shock resistance of fibrous monolithic Si_3N_4/BN ceramics, J. Eur. Ceram. Soc. 24 (2004) 2339–2347.
[7] K. Liu, C.R. Zhang, Y.D. Xiao, F. Cao, S.Q. Wang, B. Li, Synthesis of fibrous Si_3N_4–BN composites using borazine as the precursor, Mater. Sci. Eng. A 575 (2013) 48–50.
[8] K. Liu, C.R. Zhang, B. Li, S.Q. Wang, F. Cao, Synthesis of porous silicon nitride–boron nitride composites by gel-casting and PIP, J. Mater. Eng. Perform. 23 (2014) 2829–2833.
[9] S.Q. Guo, N.T. Hirosaki, Y. Yamamoto, T. Nishimura, M. Mitomo, Fracture toughness of hot-pressed $Lu_2Si_2O_7$–Si_3N_4 and $Lu_4Si_2O_7N_2$–Si_3N_4 ceramics and correlation to microstructure and grain-boundary phases, Ceram. Int. 30 (2004) 635–641.
[10] K. Liu, C.R. Zhang, B. Li, S.Q. Wang, F. Cao, Effect of pyrolysis temperature on properties of porous Si_3N_4–BN composites fabricated via PIP route, J. Mater. Eng. Perform. 22 (2013) 3684–3688.
[11] C. Ramírez, S.M. Vega-Diaz, A. Morelos-Gómez, F.M. Figueiredo, M. Terrones, M.I. Osendi, M. Belmonte, P. Miranzo, Synthesis of conducting graphene/Si_3N_4 composites by spark plasma sintering, Carbon 57 (2013) 425–432.
[12] C. Balázsi, Z. Shen, Z. Kónya, Z. Kasztovszky, F. Wéber, Z. Vértesy, L.P. Biró, I. Kiricsi, P. Arató, Processing of carbon nanotube reinforced silicon nitride composites by spark plasma sintering, Compos. Sci. Technol. 65 (2005) 727–733.
[13] M.H. Bocanegra-Bernal, J. Echeberria, J. Ollo, A. Garcia-Reyes, C. Domínguez-Rios, A. Reyes-Rojas, A. Aguilar-Elguezabal, A comparison of the effects of multi-wall and single-wall carbon nanotube additions on the properties of zirconia toughened alumina composites, Carbon 49 (2011) 1599–1607.
[14] X.M. Li, X.W. Yin, L.T. Zhang, L.F. Cheng, Y.C. Qi, Mechanical and dielectric properties of porous Si_3N_4–SiO_2 composite ceramics, Mater. Sci. Eng. A 500 (2009) 63–69.
[15] K.S. Novoselov, A.K. Geim, S.V. Morozov, D. Jiang, Y. Zhang, S.V. Dubonos, I. V. Grigorieva, A.A. Firsov, Electric field in atomically thin carbon films, Science 306 (2004) 666–669.
[16] J.C. Meyer, A.K. Geim, M.I. Katsnelson, K.S. Novoselov, T.J. Booth, S. Roth, The structure of suspended graphene sheets, Nature 446 (2007) 60–63.
[17] C. Lee, X.D. Wei, J.W. Kysar, J. Hone, Measurement of the elastic properties and intrinsic strength of monolayer graphene, Science 321 (2008) 385–388.
[18] J.T. Paci, T. Belytschko, G.C. Schatz, Computational studies of the structure, behavior upon heating, and mechanical properties of graphite oxide, J. Phys. Chem. C 111 (2007) 18099–18111.
[19] M.J. McAllister, J.L. Li, D.H. Adamson, H.C. Schniepp, A.A. Abdala, J. Liu, M. Herrera-Alonso, D.L. Milius, R. Car, R.K. Pruďhomme, I.A. Aksay, Single sheet functionalized graphene by oxidation and thermal expansion of graphite, Chem. Mater. 19 (2007) 4396–4404.
[20] S.V. Morozov, K.S. Novoselov, M.I. Katsnelson, F. Schedin, D.C. Elias, J. A. Jaszczak, A.K. Geim, Giant Intrinsic carrier mobilities in graphene and its bilayer, Phys. Rev. Lett. 100 (2008) 6602–6607.
[21] R.S. Shishir, F. Chen, J. Xia, N.J. Tao, D.K. Ferry, Room temperature carrier transport in graphene, J. Comput. Electron. 8 (2009) 43–50.
[22] K.S. Novoselov, Z. Jiang, Y. Zhang, S.V. Morozov, H.L. Stormer, U. Zeitler, J. C. Maan, G.S. Boebinger, P. Kim, A.K. Geim, Room temperature quantum Hall effect in graphene, Science 315 (2007) 1379.
[23] A.A. Balandin, S. Ghosh, D.L. Nika, E.P. Pokatilov, Extraordinary thermal conductivity of graphene: possible applications in thermal management, ECS Trans. 28 (2010) 63–71.
[24] Z. Jiang, Y. Zhang, Y.W. Tan, H.L. Stormer, P. Kim, Quantum Hall effect in graphene, Solid State Commun. 143 (2007) 14–19.
[25] T. Ramanathan, A.A. Abdala, S. Stankovich, D.A. Dikin, M. Herrera-Alonso, R. D. Piner, D.H. Adamson, H.C. Schniepp, X. Chen, R.S. Ruoff, S.T. Nguyen, I. A. Aksay, R.K. Pruďhomme, L.C. Brinson, Functionalized graphene sheets for polymer nanocomposites, Nat. Nanotechnol. 3 (2008) 327–331.
[26] S. Stankovich, D.A. Dikin, G.B. Dommett, K.M. Kohlhaas, E.J. Zimney, E.A. Stach, R.D. Piner, S.T. Nguyen, R.S. Ruoff, Graphene-based composite materials, Nature 442 (2006) 282–286.
[27] M. Koo, J.S. Bae, S.E. Shim, D. Kim, D.G. Nam., J.W. Lee, G.W. Lee, J.H. Yeum, W. Oh, Thermo-dependent characteristics of polyimide–graphene composites, Colloid Polym. Sci. 289 (2011) 1503–1509.
[28] H.Y. Song, X.W. Zha, Mechanical properties of Ni-coated single graphene sheet and their embedded aluminum matrix composites, Commun. Theor. Phys. 54 (2010) 143–146.
[29] J.Y. Wang, Z.Q. Li, G.L. Fan, H.H. Pan, Z.X. Chen, Reinforcement with graphene nanosheets in aluminum matrix composites, Scr. Mater. 66 (2012) 594–597.
[30] L.S. Walker, V.R. Marotto, M.A. Rafiee, N. Koratkar, E.L. Corral, Toughening in graphene ceramic composites, ACS Nano 5 (4) (2011) 3182–3190.
[31] J. Liu, H.X. Yan, K. Jiang, Mechanical properties of graphene platelet-reinforced alumina ceramic composites, Ceram. Int. 39 (2013) 6215–6221.
[32] P. Miranzo, C. Ramírez, B.R. Manso, L. Garzón, H.R. Gutiérrez, M. Terrones, C. Ocal, M.I. Osendi, M. Belmonte, In situ processing of electrically conducting graphene/SiC nanocomposites, J. Eur. Ceram. Soc. 33 (2013) 1665–1674.
[33] P. Rutkowski, L. Stobierski, G. Górny, Thermal stability and conductivity of hot-pressed Si_3N_4–graphene composites, J. Therm. Anal. Calorim. 116 (2014) 321–328.
[34] A. Rahman, A. Singh, S.P. Harimkar, R.P. Singh, Spark plasma sintering and characterization of graphene reinforced silicon carbide nanocomposites, in: E. Patterson, D. Backman, G. Cloud (Eds.), Composite Materials and Joining Technologies for Composites, The Society for Experimental Mechanics, Inc., California, 2012, pp. 139–146.
[35] A. Vijayaraghavan, Graphene-properties and characterization, in: R. Vajtai (Ed.), Springer Handbook of Nanomaterials, Springer, Inc., Heidelberg, 2013, pp. 50–51.
[36] R.G. Duan, G. Roebben, J. Vleugels, O. Van der Biest, Stability of intergranular phases in hot-pressed Si3N4 studied with mechanical spectroscopy and in-situ high-temperature XRD, J. Eur. Ceram. Soc. 22 (2002) 1897–1904.